Near-field model of ultrasonic array data

Alexander Velichko

Citation: AIP Conference Proceedings **1806**, 040001 (2017); doi: 10.1063/1.4974588
View online: http://dx.doi.org/10.1063/1.4974588
View Table of Contents: http://aip.scitation.org/toc/apc/1806/1
Published by the American Institute of Physics

Near-Field Model of Ultrasonic Array Data

Alexander Velichko

Department of Mechanical Engineering, University of Bristol, Bristol, BS8 1TR, UK

Corresponding author: a.velichko@bristol.ac.uk

Abstract. One method of efficiently modelling of ultrasonic array data is based on a combination of a ray-tracing approach and far-field scattering amplitude of a scatterer. This technique uses two main assumptions: all scatterers are located in the far-field from each array element and the size of each scatterer is small relative to its distance to array elements. The key part of the model is the so-called scattering matrix, which provides the amplitude and phase of scattered waves in the far-field of the scatterer. However, the far-field approximation fails when the size of the scatterer becomes comparable to its distance to array elements. In this paper a near-field model of ultrasonic array data is developed. In particular, it is shown that the near-field scattering behavior can be extracted from the scattering matrix. The applications of the model are discussed and supported with modelling examples.

INTRODUCTION

A mathematical modeling of the ultrasonic array data plays an important part in quantitative NDE. The complete model includes the excitation of the incident wave, its interaction with the scatterer and the detection of the reflected wave and can be used to assess the performance of a given array or for the interpretation of experimental results. It also can serve as a basis for developing and optimizing the imaging methods. One efficient modelling approach consists in combining a ray-tracing technique and far-field scattering amplitude of a scatterer [1]. Below this method is referred to as a far-field model and is based on two main assumptions: all scatterers are located in the far-field from each array element and the size of each scatterer is small relative to its distance to array elements. In the far-field the scatterer's behavior can be described in terms of a scattering matrix, which is defined as a far-field directivity of scattered wave for a given plane incident wave [1,2]. The scattering matrix depends on directions of propagation of incident and scattered waves and also is a function of frequency. However, the far-field approximation fails when the size of the scatterer becomes comparable to its distance to array elements. The far-field of the scatterer can be approximately estimated as:

$$F < 1, \tag{1}$$

where F is the Fresnel number,

$$F = \frac{D^2}{r\lambda}. \tag{2}$$

Here D is the size of the scatterer and r is the distance from the nominal center of the scatterer.

In this paper a near-field model of ultrasonic array data is developed. In particular, it is shown that the near-field scattering behavior can be extracted from the scattering matrix. The applications of the model are discussed and supported with modelling examples.

43rd Annual Review of Progress in Quantitative Nondestructive Evaluation, Volume 36
AIP Conf. Proc. 1806, 040001-1–040001-8; doi: 10.1063/1.4974588
Published by AIP Publishing. 978-0-7354-1474-7/$30.00

THEORY

Plane Wave Decomposition

Any time-domain signal $u(t)$ can be expressed as a linear superposition of its spectral components $u(\omega)$,

$$u(t) = \frac{1}{2\pi}\int u(\omega)e^{i\omega t}d\omega . \tag{3}$$

Therefore in this paper only time-harmonic wave fields are considered. A 2D elastic isotropic half-space is considered with Cartesian coordinate axes (x,z) defined with the z axis normal to the surface of the half-space. A transmitter element is modelled by a time-harmonic load applied to the free surface $z=0$ in a contact area with its center at $x=x_T$. The system is illustrated schematically in Fig. 1.

It is assumed that scatterer occupies the vicinity of the point $\mathbf{r}_0$. Using the integral transform technique [2] it is possible to show that the signal transmitted by the array element located at $\mathbf{r}_T = \{x_T, 0\}$ and received by the element located at $\mathbf{r}_R = \{x_R, 0\}$ can be written in the form:

$$u(\mathbf{r}_T, \mathbf{r}_R) = \int_{-\pi/2}^{\pi/2}\int_{-\pi/2}^{\pi/2} U(\gamma_T, \gamma_R)e^{-i\mathbf{k}_T\cdot(\mathbf{r}_0-\mathbf{r}_T)}e^{-i\mathbf{k}_R\cdot(\mathbf{r}_R-\mathbf{r}_0)}d\gamma_T d\gamma_R . \tag{4}$$

Here the transmit and receive wave vectors $\mathbf{k}_T, \mathbf{k}_R$ are given by

$$\mathbf{k}_T = k\{\sin\gamma_T, \cos\gamma_T\}, \quad \mathbf{k}_R = k\{-\sin\gamma_R, \cos\gamma_R\}, \tag{5}$$

and k is the wavenumber.

Expression (4) represents a plane-wave decomposition of the transmitter-receiver signal. The amplitude of plane waves is given by the function $U(\gamma_T, \gamma_R)$, which depends on the characteristics of array elements and scatterer. Note that in this expression the contribution of evanescent waves, which correspond to the complex angles, is neglected. This can be justified by the fact that evanescent waves exponentially decay with the distance from the scatterer. Moreover, the directivity of array elements results in $U = 0$ for the angles of propagation parallel to the array, $\gamma_T = \pm\pi/2$ or $\gamma_R = \pm\pi/2$.

If the transmitter and receiver elements are in the far-field of the scatterer,

$$k|\mathbf{r}_0 - \mathbf{r}_T| >> 1, \; k|\mathbf{r}_R - \mathbf{r}_0| >> 1, \tag{6}$$

and the size of the scatterer is small compared to the distance to the array,

$$F = \frac{D^2}{\min(|\mathbf{r}_0 - \mathbf{r}_T|, |\mathbf{r}_R - \mathbf{r}_0|)\lambda} < 1, \tag{7}$$

then the integral (4) can be evaluated by the stationary phase method as

$$u(\mathbf{r}_T, \mathbf{r}_R) = iU(\varphi_T, \varphi_R)\frac{\lambda}{\sqrt{R_T R_R}}e^{-ik(R_T+R_R)} . \tag{8}$$

Here (φ_T, R_T) and (φ_R, R_R) are the local polar coordinate systems defined with their origins at the center of the transmitter and receiver elements, respectively (Fig. 1).

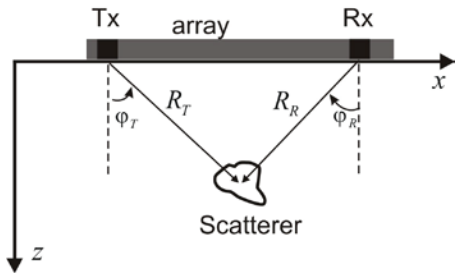

FIGURE 1. System geometry.

On the other hand, the integral transform method leads to the following far-field expression for the array data [2]:

$$u(\mathbf{r}_T,\mathbf{r}_R) = f_T(\varphi_T)S(\varphi_T,\varphi_R)f_T(\varphi_R)\frac{2\pi\lambda}{\sqrt{R_T R_R}}e^{-i\pi/4}e^{-ik(R_T+R_R)}, \tag{9}$$

where f_T is the array element directivity function and S is the scattering matrix.

By comparing (8) and (9) it can be seen that the plane wave amplitude is given by

$$U(\gamma_T,\gamma_R) = 2\pi e^{-i3\pi/4} f_T(\gamma_T)S(\gamma_T,\gamma_R)f_T(\gamma_R). \tag{10}$$

Therefore, expressions (4) and (10) provide the basis for the near-field model of ultrasonic array data. Importantly, it can be seen that the near-field data can be completely reconstructed from the far-field behavior of array elements and the scatterer.

Fourier Series Decomposition

In this section an alternative expression for the near-field array data is derived. The scattering matrix as a function of incident and scattered angles can be represented as Fourier series

$$S(\gamma_T,\gamma_R) = \sum_{m,n} S_{mn} e^{im\gamma_T} e^{in\gamma_R}, \tag{11}$$

where coefficients S_{mn} are given by

$$S_{mn} = \frac{1}{4\pi^2}\int_{-\pi}^{\pi}\int_{-\pi}^{\pi} S(\gamma_T,\gamma_R)e^{-im\gamma_T}e^{-in\gamma_R}d\gamma_T d\gamma_R. \tag{12}$$

By substituting formula (11) into (4) the following expression for the array data can be obtained

$$u(\mathbf{r}_T,\mathbf{r}_R) = \sum_{m,n} S_{mn} e^{im\varphi_T} e^{in\varphi_R} h_m(\mathbf{r}_0-\mathbf{r}_T)h_n(\mathbf{r}_R-\mathbf{r}_0), \tag{13}$$

where

$$h_m(\mathbf{r}) = \int_{-\pi/2-\varphi}^{\pi/2-\varphi} f_T(\gamma+\varphi)e^{-ikr\cos\gamma}e^{im\gamma}d\gamma, \qquad \mathbf{r} = (\varphi,r). \tag{14}$$

It can be shown that the scattering matrix can be accurately represented by a limited number of terms in the expansion (11). Below the case of the scalar wave field is considered for simplicity. For the vector wave fields the final result is the same, however, the derivation is more complicated.

Let the wave incident on a scatterer be a plane wave $\exp(-i\mathbf{k}_T\mathbf{r})$, where $\mathbf{k}_T$ is a wave vector in the incident direction, characterised by the incident angle γ_T . Each scatterer acts as a secondary source and generates a scattered wave field. This secondary source can be modelled by a distribution of forces which are applied in the area occupied by the scatterer. The response of the scatterer is described by the force distribution $f(\gamma_T,\mathbf{r})$. Then the scattered wave field can be written as the convolution integral

$$u = \int G(\mathbf{r}-\mathbf{r}')f(\gamma_T,\mathbf{r}')d\mathbf{r}' \ , \tag{15}$$

where $G(\mathbf{r}) = \frac{i}{4}H_0^{(2)}(kr)$ is 2D scalar Green's function.

Using asymptotic form of Hankel function the scattering matrix can be written as

$$S(\gamma_T,\gamma_R) = -\frac{e^{-i\pi/4}}{4\pi}\int f(\gamma_T,\mathbf{r}')e^{i\mathbf{k}_R\mathbf{r}'}d\mathbf{r}', \tag{16}$$

where $\mathbf{k}_R$ is a wave vector in the scattered direction, characterised by the scattered angle γ_R. Note that because of the linearity of the scattering problem the effective forces $f(\gamma_T,\mathbf{r})$ can be expressed as a superposition of secondary sources distributed within the scatterer

$$f(\gamma_T,\mathbf{r}) = \int g(\mathbf{r}',\mathbf{r})e^{-i\mathbf{k}_T\mathbf{r}'}d\mathbf{r}'. \tag{17}$$

Therefore, the scattering matrix can be written in the general form

$$S(\gamma_T,\gamma_R) = -\frac{e^{-i\pi/4}}{4\pi}\iint g(\mathbf{r}',\mathbf{r}'')e^{-i(\mathbf{k}_T\mathbf{r}'-\mathbf{k}_R\mathbf{r}'')}d\mathbf{r}'d\mathbf{r}''. \tag{18}$$

Using polar coordinates (r',θ'), (r'',θ'') in the integrals (18) coefficients S_{mn} can be written as

$$S_{mn} = -\frac{e^{-i\pi/4}}{16\pi^3}\int_0^{D/2} r'dr' \int_0^{D/2} r''dr'' \int_{-\pi}^{\pi} d\theta' \int_{-\pi}^{\pi} d\theta''\left[g(\mathbf{r}',\mathbf{r}'')p_m(\mathbf{r}')q_n(\mathbf{r}'')\right], \tag{19}$$

where it is assumed that the scatterer is contained in the circle of diameter D and the functions p_m, q_n are given by

$$p_m(\mathbf{r}) = \int_{-\pi}^{\pi} e^{-ikr\cos(\theta-\gamma)}e^{-im\gamma}d\gamma \ , \ q_n(\mathbf{r}) = \int_{-\pi}^{\pi} e^{ikr\cos(\theta-\gamma)}e^{-in\gamma}d\gamma \ . \tag{20}$$

Using the relationship

$$J_m(z) = \frac{e^{-im\pi/2}}{2\pi}\int_{-\pi}^{\pi} e^{iz\cos\gamma}e^{im\gamma}d\gamma, \tag{21}$$

where J_m is Bessel function, and the asymptotic of the Bessel function for large positive orders,

$$J_m(z) \approx \frac{1}{\sqrt{2\pi m}}\left(\frac{ez}{2m}\right)^m, \tag{22}$$

the expression (19) can be estimated as

$$\left|S_{mn}\right| \le const\frac{D^4}{\left|mn\right|^{3/2}}\left(\frac{\pi eD}{2\lambda|m|}\right)^m\left(\frac{\pi eD}{2\lambda|n|}\right)^n. \tag{23}$$

The relationship (23) shows that as $|m,n| \to \infty$ the coefficients S_{mn} abruptly tend to zero and the scattering matrix can be efficiently represented by a limited number of terms in the expansion (11) $|m,n| \le N$, where N depends on the size of the scatterer,

$$N \approx \frac{\pi eD}{2\lambda} + N_0, \tag{24}$$

where N_0 is the number of terms for sub-wavelength scatterers, $D << \lambda$.

MODELING EXAMPLES

The specifications of a commercial 64-element array (manufactured by Imasonic) were used for the modeling. The array has an element pitch of 0.63 mm and a total length of 40 mm. The simulated specimen was aluminum with a longitudinal wave velocity of 6320 m/s. The transmitted signal was a Hanning windowed toneburst with a centre frequency of 5 MHz.

In order to illustrate the performance of the near-field model the array data for three different scatterers were simulated. The geometry of the scatterers is schematically shown in Fig. 2. The first scatterer is a straight crack oriented parallel to the array. In this case the scattering matrix was calculated using semi-analytical method [3], which is based on the boundary integral equation method. Another scatterer represents a circular hole of 6.3 mm (5 λ) diameter with a rough surface breaking crack. The scattering matrix was calculated using efficient Finite Element method [4]. Note that once the scattering matrix of the scatterer is known then the array data for arbitrary orientation of this scatterer can be easily modelled. In this section two orientations of the surface breaking crack are considered: parallel to the array and normal to the array (Fig. 2b,c). Finally, the simulated transmit-receive array data was converted to the images using the Total Focusing Method and the images obtained using far-field model and near-field model were compared. The distance *r* in formula (2) for the Fresnel number in all cases was calculated as a minimum distance between the nominal center of the scatterer (center of the crack for the straight crack and center of the hole for the hole with the crack) and the array.

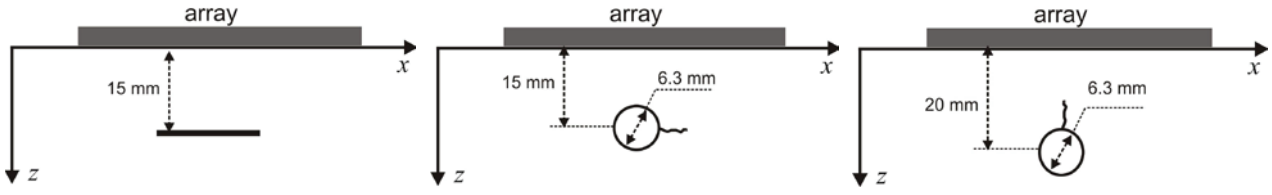

(a) (b) (c)

FIGURE 2. Geometry of the scatterers. (a) Straight crack; (b),(c) Circular hole with rough surface-breaking crack.

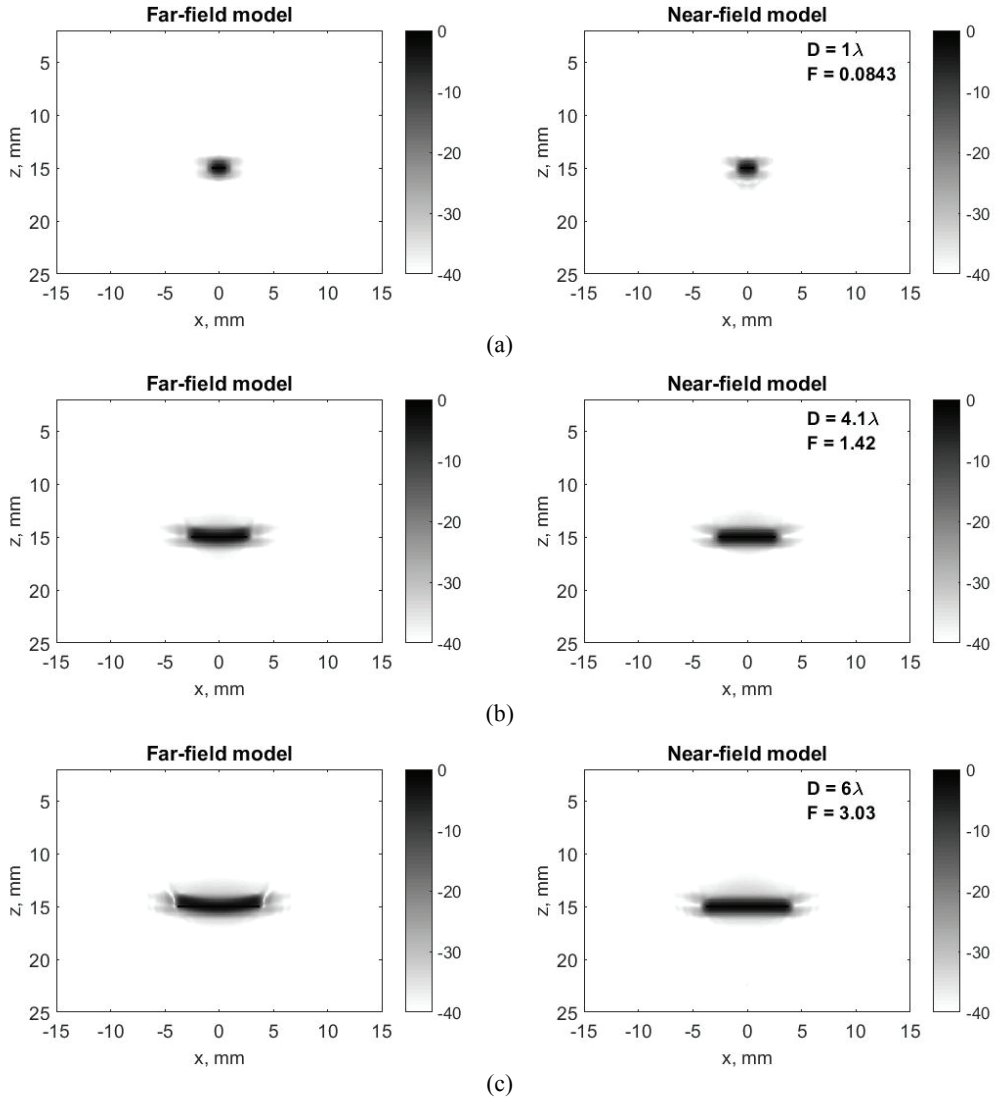

FIGURE 3. TFM images of straight crack for the crack size (a) 1λ; (b) 4.1λ; (c) 6λ. Dynamic range is in dB.

Figure 3 shows TFM images for the straight crack. It can be seen that the near-field scattering behavior becomes important when the Fresnel number F~1.4. For large cracks the far-field model produces an image which is curved towards the array.

Figure 4 shows TFM images for the circular hole with the rough surface-breaking crack oriented parallel to the array. It is seen that for this particular configuration the far-field model becomes inaccurate even for small cracks about wavelength size. Figure 5 shows images for the circular hole with the rough surface-breaking crack oriented normal to the array. In this case differences between the far-field and near-field models become visible for cracks greater than 2.5 λ. Note that in this cases the size of the scatterer in the Fresnel number was taken as a sum of the hole diameter and crack length.

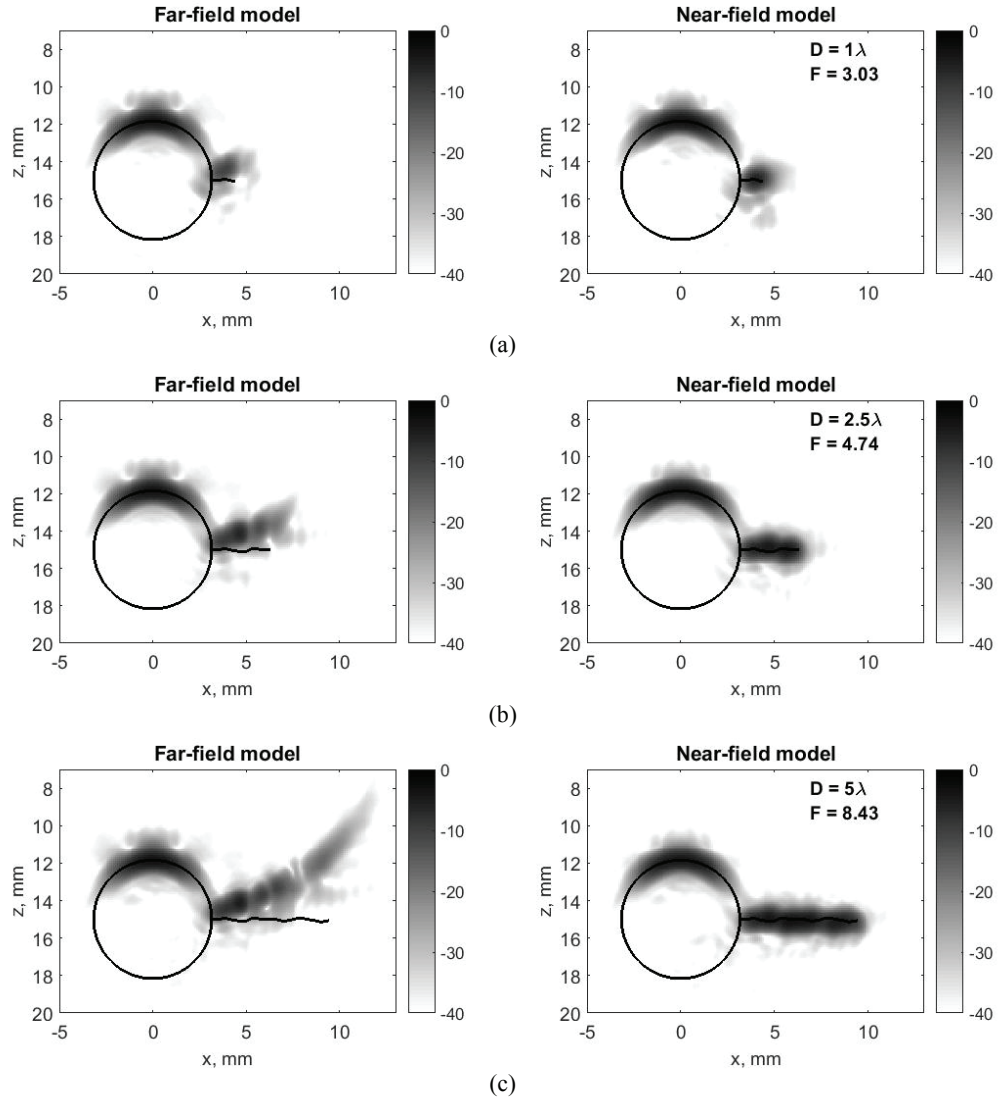

FIGURE 4. TFM images of circular hole with rough surface-breaking crack parallel to the array for the crack size (a) 1 λ; (b) 2.5 λ; (c) 5 λ. Parameter *D* corresponds to the crack length. Scatterer size for the Fresnel number is calculated as a sum of hole diameter and crack length. Dynamic range is in dB.

CONCLUSION

In this paper the near-field model of ultrasonic array data has been developed. The model can be used for modelling of ultrasonic response from large scatterers (defects or structural features) located close to the array, when the distance from the scatterer to the array is compared to the scatterer size. The model is based on a plane wave decomposition of incident and scattered wave fields. It has been shown that the amplitude of plane waves in this decomposition is directly proportional to the product of array element directivity function and scattering matrix of the scatterer. Therefore, the near-field scattering behaviour can be extracted from the far-field scattering matrix. In general near field effects become important when Fresnel number $F \sim 1$. However, the exact value strongly depends on the scattering behaviour.

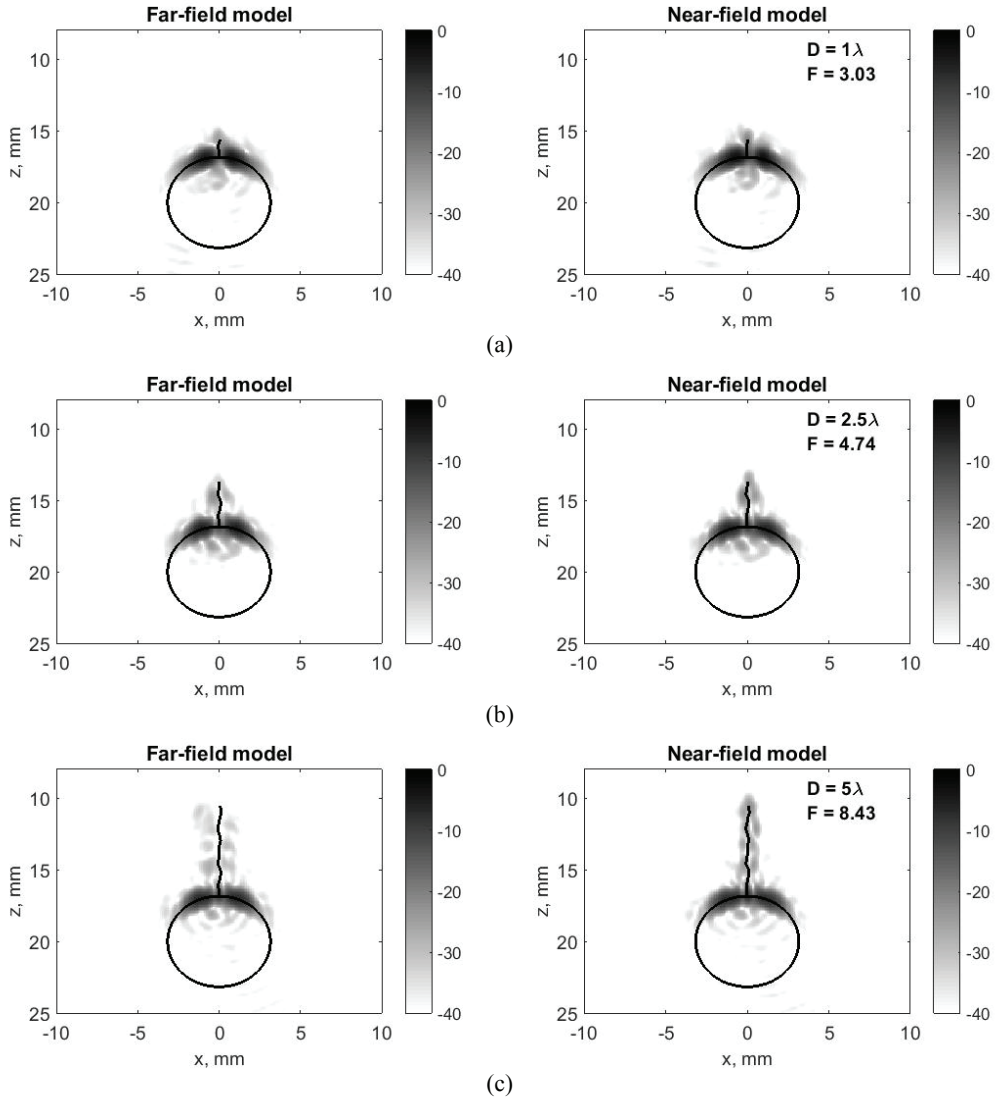

FIGURE 5. TFM images of circular hole with rough surface-breaking crack normal to the array for the crack size (a) 1 λ; (b) 2.5 λ; (c) 5 λ. Parameter *D* corresponds to the crack length. Scatterer's size for the Fresnel number is calculated as a sum of hole diameter and crack length. Dynamic range is in dB.

REFERENCES

1. J. Zhang, B. W. Drinkwater, P. D. Wilcox, A. J. Hunter, NDT&E Int., **43**, 123-133 (2010).
2. A. Velichko and P. D. Wilcox, IEEE Trans. Ultrason. Ferroelectr. Freq. Control, **56**(11), 2492–2503 (2009).
3. E. Glushkov, N. Glushkova, A. Ekhlakov, and E. Shapar, Wave Motion, **43**(6), 458–473 (2006).
4. A. Velichko, P. D. Wilcox, "Efficient finite element modelling of elastodynamic scattering with non-reflecting boundary conditions", in *Review of Progress in Quantitative Nondestructive Evaluation*, eds. D. O. Thompson and D. E. Chimenti (American Institute of Physics 1430, Melville, NY) **31**, 142–149 (2012).